



Politecnico di Torino

A.Y. 2025/2026

Master degree in Automotive Engineering

Additive and design for additive

Re-design of Ducati V4S steering plate for AM

Students:

Emanuele Landolina (S349706)

Walter Maggio (S343988)

Giuseppe Maria Marchese (S348145)

Marcello Marrella (S346927)

Contents

Contents	i
1 Introduction	1
2 Loads evaluation	3
2.1 Braking case	4
2.2 Cornering case	4
2.3 Bump impact	5
2.4 Bolts pretension	6
2.5 Model validation	6
2.5.1 Methodology	6
2.5.2 Braking load case results	8
2.5.3 Cornering load case results	9
2.5.4 Final outcome of the validation	10
3 Geometry Definition	11
3.1 Pre-processing	11
3.2 Topology Optimization	12
3.3 Geometry Finishing and Final Shape	15
3.4 Geometry with Machining Allowance	16
4 Printing and Manufacturability	18
4.1 Manufacturing Strategy and Setup	18
4.1.1 Machine Specification (EOS M 400-4)	18
4.1.2 Process Parameters	19
4.1.3 Orientation and Nesting Strategy	19
4.1.4 Hybrid Support Structure Design	20
4.2 Process Simulation Methodology	21
4.2.1 Process Calibration	21
4.2.2 Final Analysis Configuration	21
4.3 Results and Structural Validation	22

4.3.1	AlSi10Mg Analysis Results	22
4.3.2	A20X Analysis Results	23
4.3.3	Structural Integrity Verification	24
5	Performance Analysis	26
5.1	FEM analysis on AlSi10Mg Part	26
5.2	FEM analysis on A20x Part	28
5.3	FEA Results comparison	30
5.4	Weight evaluation	31
5.5	Final considerations	31
6	Post-Processing	32
6.1	Post-Processing Strategy	32
6.2	Custom Fixtures and Manufacturing Workflow	33
6.2.1	Operational Workflow	33
7	Cost analysis	37
7.1	Production Rate and Lead Time Assessment	39
8	Conclusion	40

Chapter 1

Introduction

This report presents a comprehensive feasibility study and re-design regarding the production of the upper steering plate for the Ducati V4 S (Superleggera).



Figure 1.1: Ducati V4 S motorcycle

Traditionally, this component is CNC machined from a solid block of Anticorodal aluminum alloy, weighing 400 grams. The primary objective of this project is to evaluate the transition from this conventional subtractive process to an Additive Manufacturing (AM) workflow, targeting a production volume of 500 parts per year. To design the new component, topology optimization was performed to maximize stiffness while reducing mass. The structural integrity of the optimized design was verified through FEM analysis, ensuring the component could withstand the complex load cases experienced during riding. A comparative analysis of two distinct high-performance materials suitable for AM, *A20X* and *AlSi10Mg*, was performed.

The report evaluates the mechanical performance and manufacturability of both alloys to determine the most suitable candidate for this application. Furthermore, the study

addresses the post-processing phase, detailing a strategy for part orientation and support design to ensure printability and geometrical accuracy. Finally, the report discusses a detailed cost analysis. This economic evaluation contrasts the AM production chain with the traditional CNC process, providing a final assessment on the technical and financial feasibility of the re-design.

Chapter 2

Loads evaluation

The upper steering plate of the Ducati V4 S is a critical structural component subjected to a complex variety of loads resulting from road conditions, riding dynamics, and structural constraints. According to the project specifications, these loads include vertical forces from the rider and motorcycle weight, lateral forces during cornering, torsional stresses from steering manoeuvres, and significant longitudinal loads induced by braking and acceleration.

To perform a reliable topology optimization and FEM analysis, it was necessary to translate these real-world dynamic conditions into static load cases. Consequently, some assumptions and approximations were made to simplify the physical model without compromising the accuracy of the structural evaluation:

- the connection between the fork tubes and the steering plate is assumed to be perfectly rigid for the purpose of force transmission;
- the vertical forces are split in half between the upper and lower steering plates;
- dynamic peaks caused by road irregularities are accounted for by applying safety factors;
- the mass distribution of the rider and bike is assumed to be constant during the static snapshots of braking and cornering.
- the constraint is applied to the central pin, with all the degrees of freedom constrained.

Based on these assumptions, the analysis focuses on the three most critical scenarios identified as the dimensioning load cases: Braking, Cornering and Bump impact.

2.1 Braking case

Braking represents one of the most severe conditions for the steering assembly. During hard braking, significant longitudinal forces are transmitted through the forks to the steering plate. Simultaneously, the weight transfer towards the front of the motorcycle generates a high vertical compressive load. In this scenario, the resulting forces acting on the steering plate :

- Vertical Force ($F_{z,braking}$): 980N
- Horizontal/Longitudinal Force ($F_{x,braking}$): 3800N

These forces result in a bending moment on the steering pin and the surrounding supports. They are applied to the model as shown in figure 2.1.

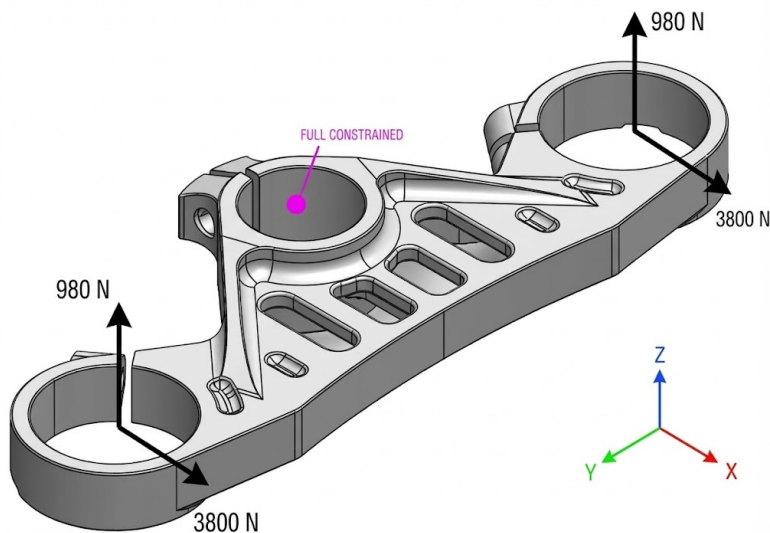


Figure 2.1: Braking cases

2.2 Cornering case

During high-speed cornering, the motorcycle is subjected to lateral loads resulting from the interaction between the tires and the ground and the centrifugal force. For the simulation, the calculated load components are:

- Vertical Force ($F_{z,braking}$): 1500N
- Horizontal/Longitudinal Force ($F_{x,braking}$): 1000N

These forces, which generate bending and torsional moments, are applied as shown in figure 2.2

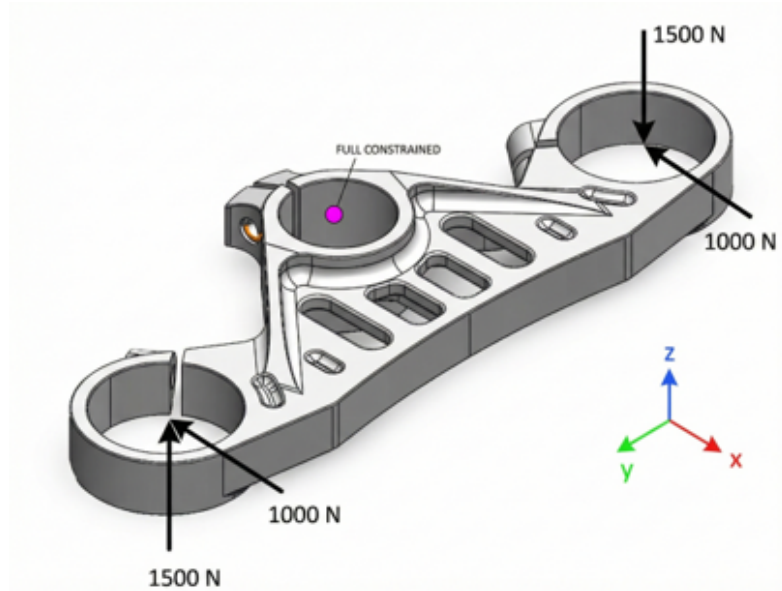


Figure 2.2: Cornering cases

This load case is critical for ensuring the torsional rigidity of the plate, which is essential for maintaining steering precision and rider feedback.

2.3 Bump impact

This case focuses on a critical, high-magnitude dynamic load case: the transient impact generated by forces from road obstacles, capable of creating sudden stress peaks within the steering plate structure. This transient should be modelled as an impulsive force, but for sake of simplicity it has been converted as a static force by doubling it. The hypotheses are:

- the bump is 5 cm high;
- the collision happens at 30 km/h.
- static load is twice the actual impact load.
- the vertical loads are damped about 60% by the forks and tyre.

These forces, which generate bending and torsional moments, are applied as shown:

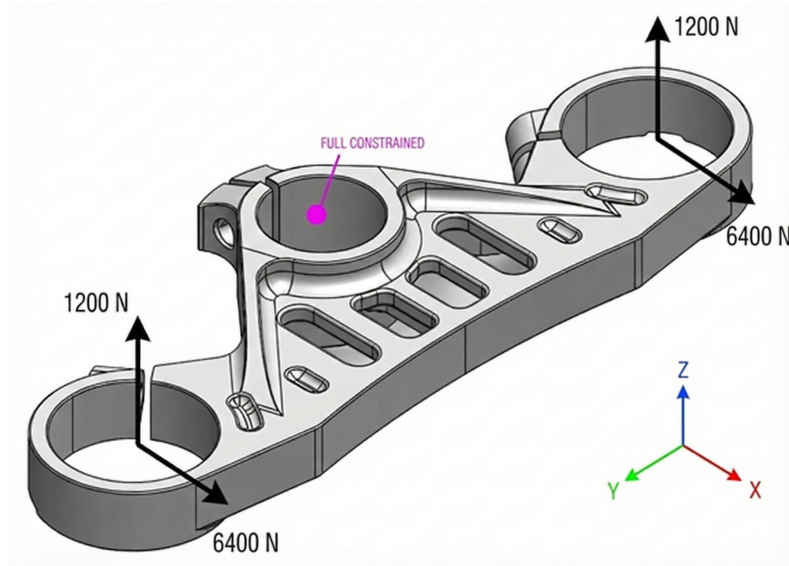


Figure 2.3: Bump case

2.4 Bolts pretension

The bolts pretension has been applied with static loads. In particular, two tightening forces in the same direction but opposite direction of 7000N that correspond to a bolt tightening of 22 Nm.

2.5 Model validation

Before proceeding with the design of the Additive Manufacturing component, a reverse engineering process was conducted to validate the calculated load cases. The original CNC-machined component (Anticorodal aluminum alloy, 400g) was modeled and subjected to an FEM analysis using the loads derived in Sections 2.1 and 2.2. The analysis has been conducted with the Altair Hypermesh software.

2.5.1 Methodology

The FEM model has been produced with the following steps:

1. creation of nodes into the holes (for loads and constraints);
2. geometry cleanup (for unnecessary geometries);
3. generation of 2D mesh of 1mm (mixed quad and trias);
4. generation of 3D mixed mesh of 1mm;

5. generation of rigids with RBE3 to simulate the distribution of loads and constraints;
6. application of loads and constraints
7. creation of material and property cards and application to the 3D mesh.
8. Creation of the loadsteps

The final model ready to be simulated is shown.



Figure 2.4: Original model meshed with loads

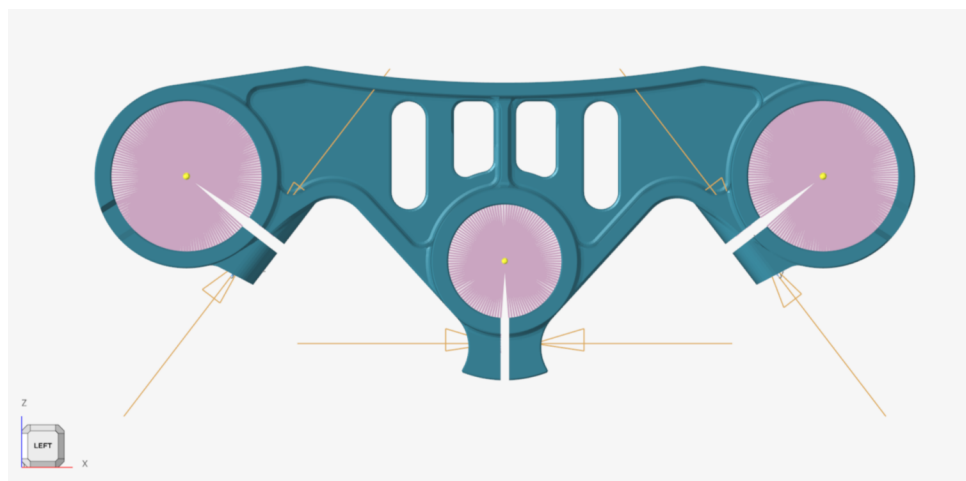


Figure 2.5: Original model meshed with rigids and bolts preloads

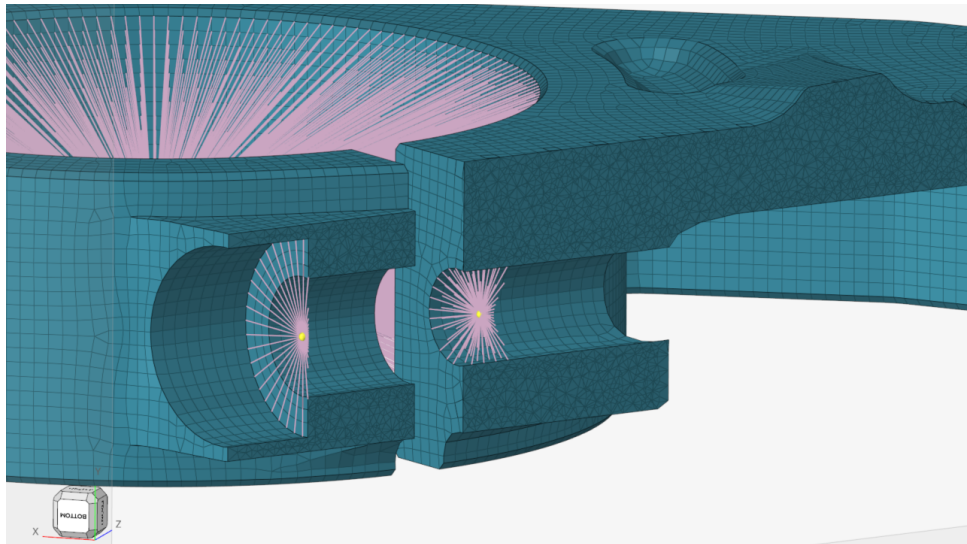


Figure 2.6: Rigid elements for bolts section cut

In the last figure (2.6) a section cut is reported, to show the particular of the rigid elements used to distribute the load of a bolt. The head of the bolt is simulated using the nodes on the surface where the force is spread, while the threads are simulated collecting the nodes on the surface of the hole, with a depth of 4 mm.

A similar thing has been done for the forks pins (figure 2.5), where the independent node, the one at the center of the pins, is connected with the RBE3 to the internal face of the holes.

2.5.2 Braking load case results

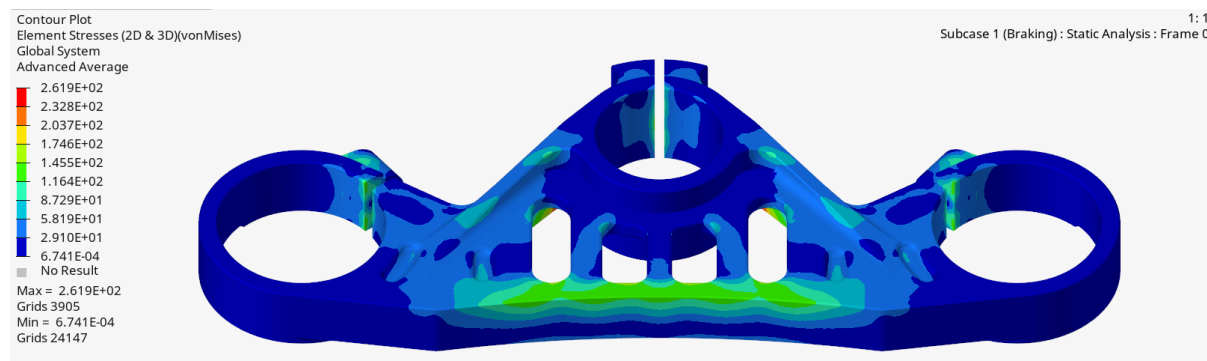


Figure 2.7: Braking loadcase (top view)

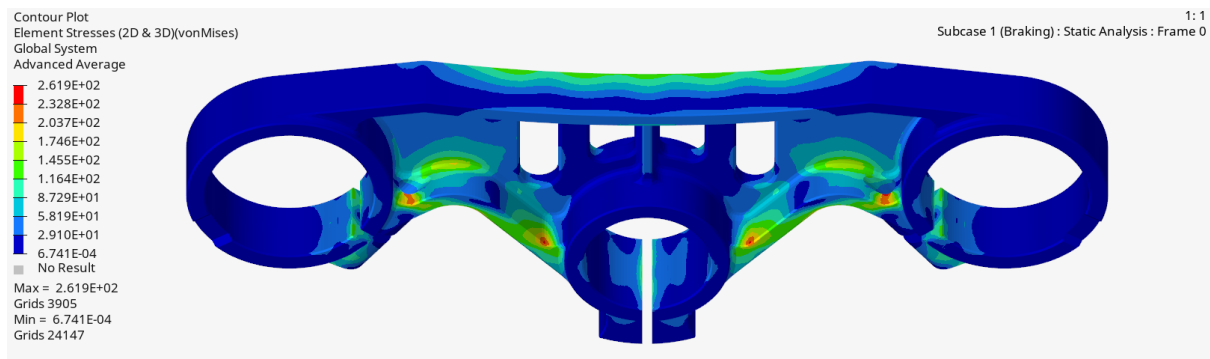


Figure 2.8: Braking loadcase (bottom view)

As it is possible to see in figure 2.7 the original steering plate has almost no criticalities, being overall under the yielding stress with a safety factor. But still the value in the legend report high maximum stresses. As shown in figure 2.8, there are some critical spots where the stresses are concentrated, providing some hint for the optimization.

2.5.3 Cornering load case results

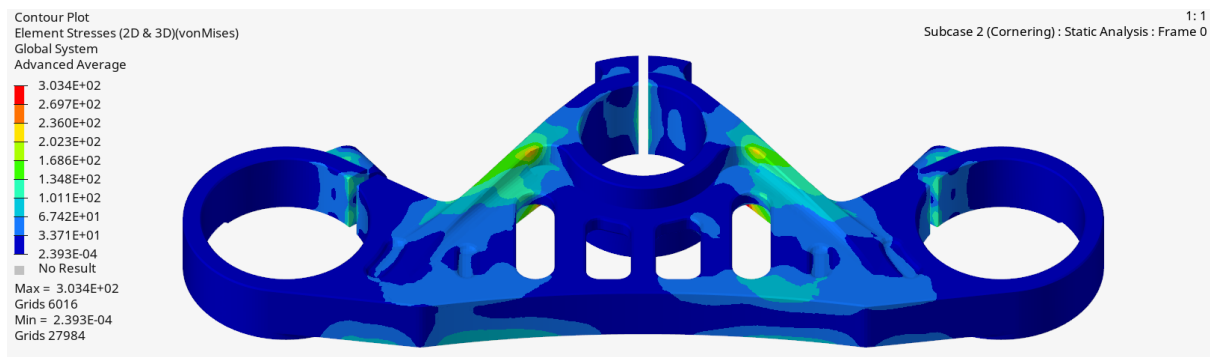


Figure 2.9: Cornering loadcase (top view)

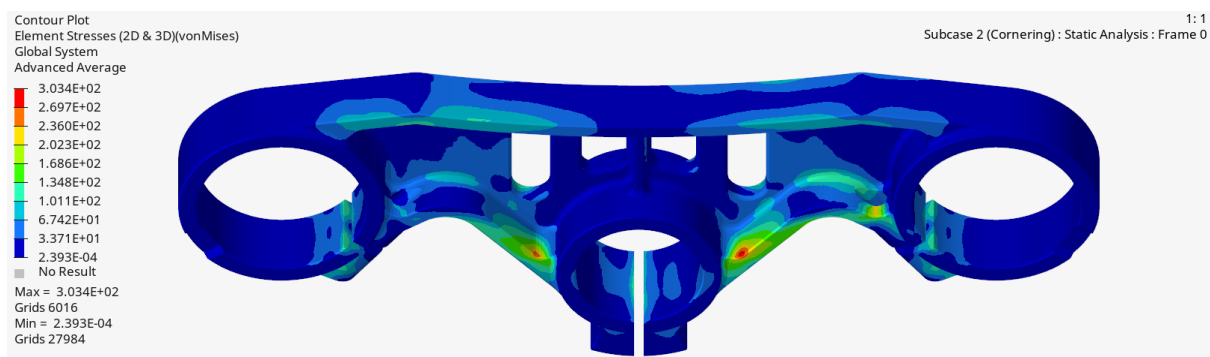


Figure 2.10: Cornering load case (bottom view)

In the cornering load case more stress is applied to the steering plate due to the torsional movement and it is clearly asymmetric, as expected from the theoretical model. For this

reason in figure 2.10 a critical spot is visible on the bottom-right part of the plate.

2.5.4 Final outcome of the validation

In general the steering plate is valid and can resist well against the subjected load cases, thus validating the theoretical model.

The analysis demonstrated also that there is room for improvement both for the management of the loads and for the reduction of weight.

An in-depth analysis of the results and a comparison with the optimized parts will be reported in section 5.3.

Chapter 3

Geometry Definition

3.1 Pre-processing

The initial phase involved preparing the component geometry to define the effective design space for optimization. As the original component was manufactured via CNC machining from a solid block of aluminum alloy (Anticorodal) and featured numerous lightening pockets, the geometry was unsuitable for direct topology optimization.

The primary pre-processing step required converting the existing plate into a solid design volume by infilling the internal cutouts. This conversion ensured that the optimization algorithm (Altair Inspire) could freely remove material from any point within the volume, maximizing the potential for mass reduction and structural efficiency. Furthermore, critical interfaces and functional requirements were addressed; specifically, the refinement of existing radii and fillets necessary for efficient stress distribution was ensured.

Crucially, a functional verification of the final envelope was performed. This confirmed that the maximum design space used for optimization did not interfere with adjacent components or kinematic constraints, particularly during maximum steering angle maneuvers of the Ducati V4 S.

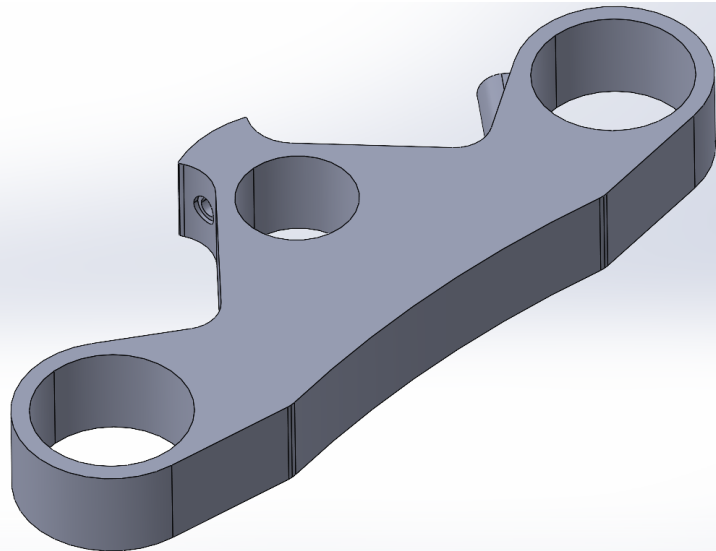


Figure 3.1: Prepared component for topology optimization

A key design decision was to retain the bolt holes. This served two purposes: first, to maintain the bolt reference axes for post-processing operations, and second, to define that volume as a *non-design space*. This constraint prevents the optimization algorithm from placing material in zones that must remain open, thereby avoiding structural conflicts during the manufacturing and assembly phases.

3.2 Topology Optimization

The material optimization of the steering plate was conducted using Altair Inspire software. The process aimed to determine the most efficient material distribution based on the validated boundary conditions established in the Load Evaluation chapter.

First, the fork clamp holes and the steering stem hole were defined as non-design zones to preserve material in these critical interfaces. A distinction was made between the two materials regarding the non-design space padding (offset):

- **AlSi10Mg:** Offset set to 5 mm from the inner surface.
- **A20x:** Offset reduced to 3 mm.

This differentiation accounts for the superior mechanical properties of the A20x material, which allows for reduced wall thickness without compromising structural integrity. For both models, a symmetry plane was enforced to ensure the left and right sides of the triple clamp were geometrically identical.

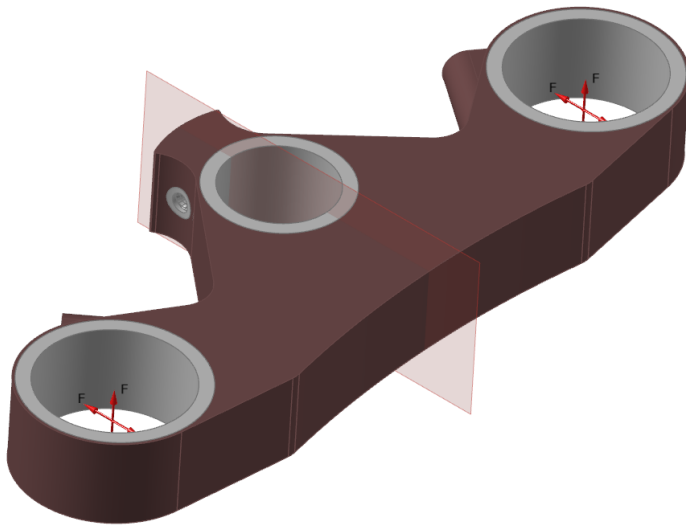


Figure 3.2: AlSi10Mg model preparation for topology optimization

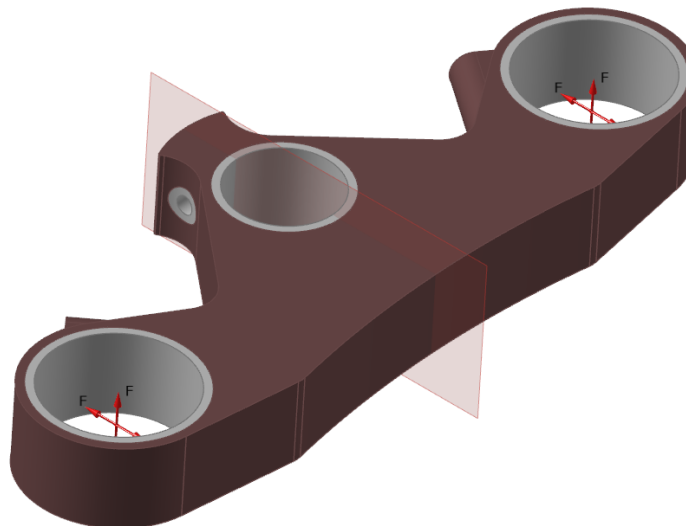


Figure 3.3: A20x model preparation for topology optimization

The component was optimized to minimize mass while maintaining the necessary structural strength to guarantee a safety factor of 1.2. The topology optimization parameters are summarized in Table 3.1.

Parameter	Value
Objective	Minimize mass
Stress constraints	Min. Safety Factor: 1.2
Frequency constraints	None
Optimization Speed	Faster

Table 3.1: Topology optimization settings

After several iterations, the following results were obtained:

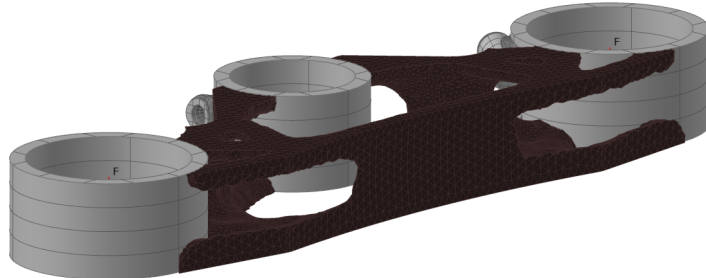


Figure 3.4: AlSi10Mg topology optimized part

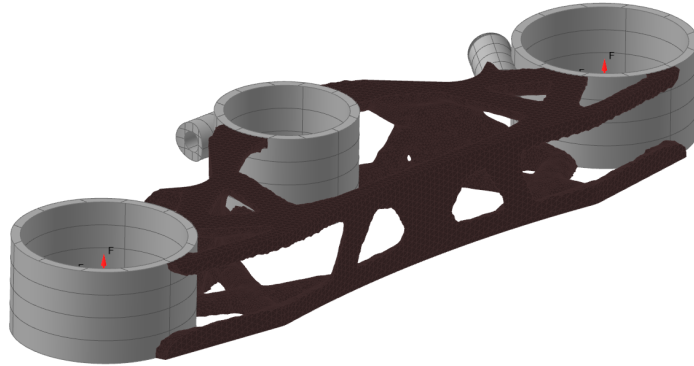


Figure 3.5: A20x topology optimized part

From a preliminary analysis, it is evident that the A20x component requires significantly less material than the AlSi10Mg counterpart. This is attributable to the notably higher yield strength of the A20x alloy, allowing for a greater reduction in mass.

However, the raw output of topology optimization inherently results in a jagged and irregular surface. Therefore, a geometry reconstruction process was performed to smooth the surfaces and blend the optimized material with the non-design regions, thereby improving surface quality, structural continuity, and aesthetics. To execute this step, the *Fit* tool within the PolyNURBS module was utilized. The results are presented in the following figures.

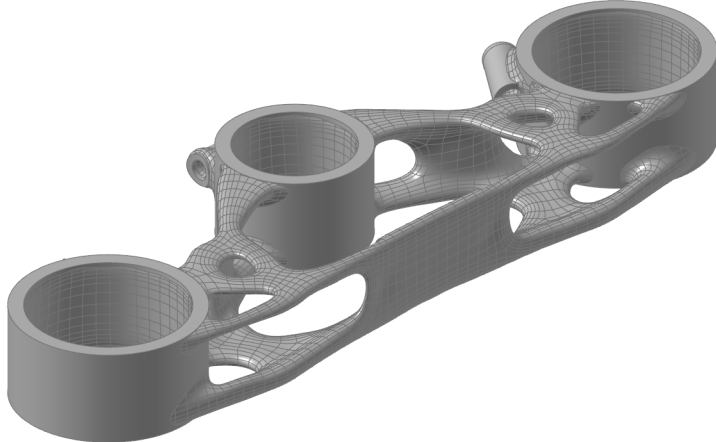


Figure 3.6: AlSi10Mg refined topology optimized part

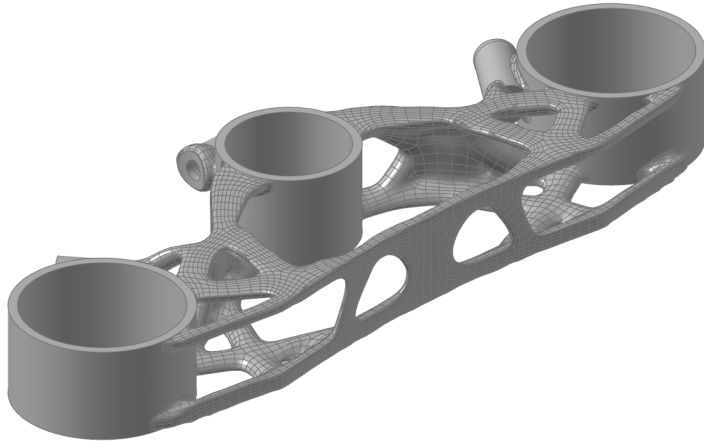


Figure 3.7: A20x refined topology optimized part

The resulting optimized geometry underwent a preliminary static validation via FEM analysis. This critical step verified that the final design successfully withstood the combined maximum stresses induced by all applied load scenarios. The component was deemed acceptable only after confirming that the maximum equivalent stress (σ_{vM}) remained below the material yield strength (σ_y), ensuring an adequate safety factor across the entire structure. Furthermore, stiffness was verified to ensure deformations remained within an acceptable range to guarantee steering precision.

Following this validation, the geometry was finalized and prepared for the conclusive FEM analysis, the results of which are presented in the chapter 5.

3.3 Geometry Finishing and Final Shape

Upon exporting the optimized topology from Inspire, the geometry was imported into SolidWorks to perform the final operations required to achieve the production-ready

shape. First, the bolt holes were reconstructed and blended with the main body to enhance local structural strength.

Subsequently, to further decrease mass without compromising structural resistance, two relief slots were opened on the outer periphery of the fork clamp housings. As a final operation, the original vertical slots were reintroduced to enable the fork clamping mechanism. The final renderings are presented below:



Figure 3.8: Rendering of final AlSi10Mg part

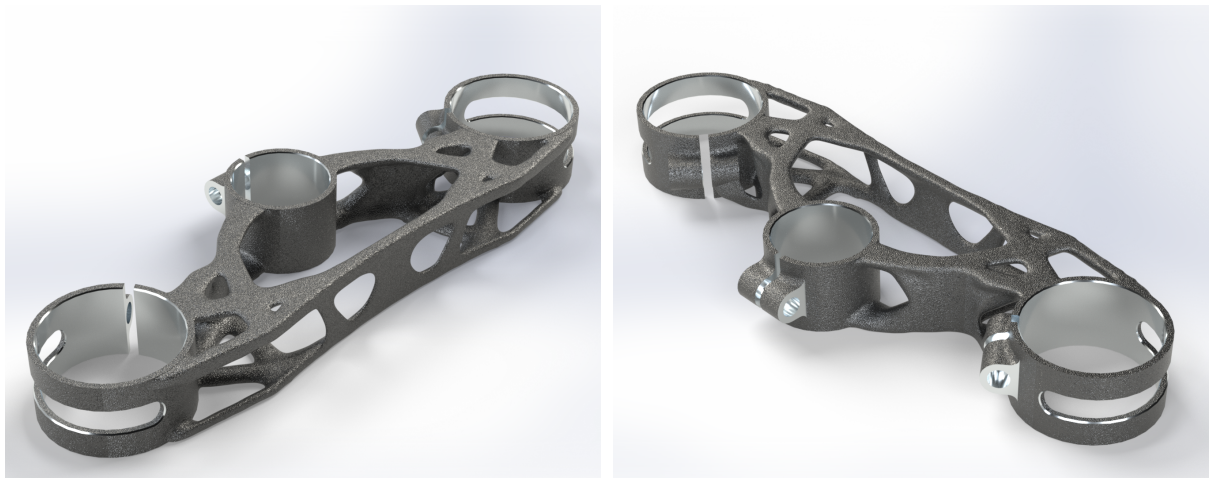


Figure 3.9: Rendering of final A20x part

3.4 Geometry with Machining Allowance

To prepare the component for manufacturing, the geometry was modified in SolidWorks to include machining allowances. These allowances are necessary to compensate for thermal distortions characteristic of the Additive Manufacturing (specifically SLM) process and to ensure sufficient material is available for post-process machining to achieve tight geometric tolerances.

A machining allowance of 1.5 mm was added to the clamping holes. Additionally, the bolt hole diameters were reduced to 5 mm. This reduction serves two purposes: it allows the holes to be printed without internal supports, and it provides the necessary material stock for the subsequent tapping operations to create the threads. The resulting geometries are shown in the following images:

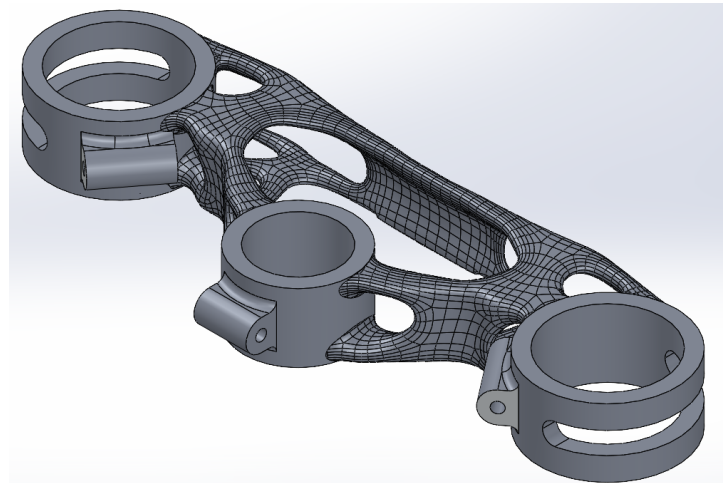


Figure 3.10: AlSi10Mg part with machining allowance

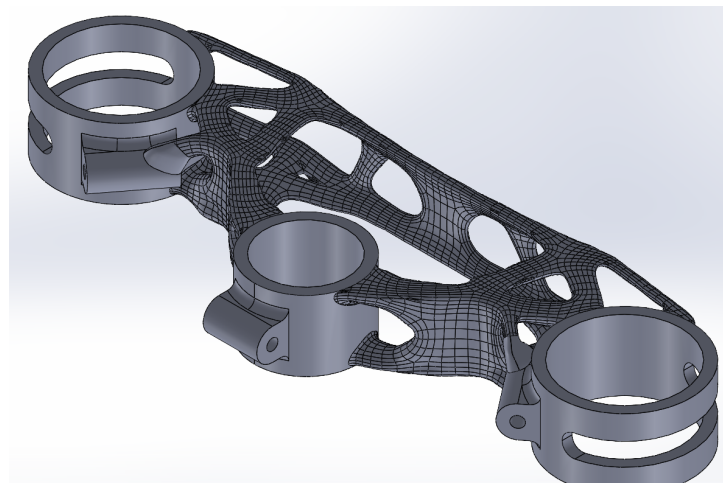


Figure 3.11: A20x part with machining allowance

Chapter 4

Printing and Manufacturability

Following the topology optimization phase conducted in Altair Inspire and the subsequent geometry reconstruction in SolidWorks, the finalized CAD model of the Ducati V4S Superleggera steering plate was prepared for the additive manufacturing simulation.

This phase is critical to ensure the manufacturability of the optimized lightweight design, reconciling the complex organic geometries with the physical constraints of the Laser Powder Bed Fusion (LPBF) process.

4.1 Manufacturing Strategy and Setup

The definition of the production environment involves selecting the appropriate hardware, defining the optimal process parameters, and establishing a robust build strategy. This foundation is essential to ensure the feasibility of the simulation model.

4.1.1 Machine Specification (EOS M 400-4)

The production simulation was set up for the **EOS M 400-4** system. This machine was selected for its large build volume ($400 \times 400 \times 400$ mm), which is a crucial factor for the chosen industrialization strategy, allowing for high-density nesting of multiple components.

The key feature of the chosen manufacturing system is the **Quad-Laser Configuration**. The system utilizes four 400-watt Yb-fiber lasers operating simultaneously. This capability is particularly relevant for the chosen vertical orientation strategy: although the significant Z-height increases the number of layers, the multi-laser exposure reduces the scanning time per layer, mitigating the impact on the total build duration.

4.1.2 Process Parameters

While the simulation relies on a calibrated inherent strain model, the physical production on the **EOS M 400-4** requires a specific parameter set ("exposure strategy") optimized for the Aluminum alloy.

For this project, high-productivity but still optimal parameter set has been selected to complement the nesting strategy. The key process variables defined for the build job are listed in Table 4.1. These settings govern the interaction between the laser energy and the powder bed, directly influencing the density and mechanical properties of the final components.

Process Parameter	Value
Layer Thickness	0.08 mm
Scan Speed	1300 mm/s
Recoating Time	13.0 s

Table 4.1: Manufacturing process parameters defined for the EOS M 400-4 production run.

4.1.3 Orientation and Nesting Strategy

The primary objective of this study was to define the optimal orientation of the component within the build volume. Unlike prototyping scenarios where speed is the sole priority, this project addressed a multi-objective optimization problem focusing on **industrial productivity, stress mitigation, and cost amortization**.

Vertical Alignment and Batch Production The orientation strategy adopted a "Maximum Building Height" approach, aligning the component primarily along the Z-axis. While this maximizes the recoating steps, it drastically minimizes the projected area on the XY plane. This minimal footprint allowed for the high-density nesting of **12 steering plates** in a single build cycle. This achievement has substantial economic implications: the fixed costs associated with machine setup, inert gas consumption, and operational time are amortized across a larger batch, significantly reducing the per-unit manufacturing cost compared to a horizontal orientation.

Stress Mitigation (5° Tilt) Although the alignment is vertical, the component was not positioned perfectly parallel to the build direction. A strategic inclination of approximately **5 degrees** was applied. This adjustment serves two critical functions:

1. **Thermal Management:** It prevents large cross-sectional areas from being sintered simultaneously in a single layer, ensuring a more gradual thermal transition and reducing the risk of local overheating.

2. **Recoater Safety:** It avoids long, continuous edges striking the recoater blade abruptly, which could lead to print failures or layer shifts.

4.1.4 Hybrid Support Structure Design

To ensure successful printability of the complex, topology-optimized geometry while facilitating post-processing, a hybrid support strategy employing three distinct structural types was developed.

1. **Base Anchoring Supports (Solid):** The lowest sections of the component, responsible for anchoring the part to the build plate, are subjected to the highest thermal pull-up forces. Therefore, solid volume supports were utilized in these foundational layers to guarantee maximum rigidity and resistance against detachment.
2. **Functional Hole Supports (Tree Structure):** The critical functional surfaces of the three holes (for crowning and forks) required careful consideration. External "tree" type supports were applied to these areas (parameters in Table 4.2). Tree supports offer excellent stability and stress reduction during the build. Crucially, their branching design results in minimal contact points with the component surface, significantly facilitating the removal during post-processing and preserving the dimensional accuracy of the holes.

Parameter	Value
Support Type	Tree
Spacing	1.0 mm
Distance to Contour	0.4 mm
Pattern Angle	0.0 deg

Table 4.2: Parameters for Functional Hole Supports (Tree Type).

3. **General Body Supports (Diamond Pattern):** For the majority of the overhanging regions defined by the organic shape of the plate, a cellular support structure with a diamond pattern was selected. As detailed in Table 4.3, this pattern provides necessary mechanical support during printing while optimizing material usage through a cell-based subdivision strategy.

Parameter	Value
Support Type	Diamond (Block)
Distance to Contour	0.4 mm
Pattern Angle	0.0 deg
Min Cell Size	2.0 mm
Max Subdivision Levels	2.0
Min Smallest Cells	3.0

Table 4.3: Parameters for General Body Supports (Diamond Pattern).

4.2 Process Simulation Methodology

To ensure high fidelity in the manufacturing simulation, the **Inherent Strain** method was employed. Unlike transient thermal analyses, which are computationally prohibitive for large batches, this approach predicts residual stress and deformation based on a pre-calculated strain profile, requiring a specific calibration to match the physics of the process.

4.2.1 Process Calibration

Prior to the full steering plate analysis, a calibration routine was executed using a standard cantilever beam specimen. This step is essential to correlate the simulation solver with the physical behavior of the material (Aluminum AlSi10Mg or Aluminum A20X) under the specific layer deposition conditions.

As illustrated in the calibration setup, the following parameters were imposed to generate the strain tensors:

- **Powder Layer Thickness:** 0.08 mm
- **Reference Deformation (D_1):** 1.0 mm

This procedure generated a dedicated calibration file, which acts as the physical constitutive model for the subsequent analysis.

4.2.2 Final Analysis Configuration

For the manufacturing simulation of the full steering plate batch, the previously generated calibration file was imported into the solver. The analysis was configured using a Voxel Mesh approach to handle the complex topology-optimized geometry.

Crucially, the **Support Thickness** in the simulation was explicitly set to 0.2 mm. This value is not arbitrary but was selected to align with the minimum feature size and

laser spot capabilities of the EOS M 400-4, ensuring that the simulated stiffness of the supports accurately reflects the real mechanical behavior of the printed structures.

The complete simulation parameters are summarized in Table 4.4.

Simulation Parameter	Value
Analysis Type	Inherent Strain
Mesh Type	Voxel
Element Size	1.0 mm
Powder Layer Thickness	0.08 mm
Support Thickness	0.2 mm

Table 4.4: Configuration parameters used for the Altair Inspire Print Analysis.

4.3 Results and Structural Validation

Following the definition of process parameters and support strategies, a comprehensive thermo-mechanical simulation was conducted. This step is pivotal to predict the behavior of the component during the layer fusion process, specifically to identify potential risks of cracking, delamination, or excessive geometric distortion caused by the accumulation of residual stresses.

The analysis was performed on the two distinct topology-optimized geometries derived for the candidate materials: **AlSi10Mg** and **A20X**. For both cases, the Von Mises yield criterion was applied to evaluate the stress distribution within the part and the support structures.

4.3.1 AlSi10Mg Analysis Results

The first simulation run focused on the AlSi10Mg steering plate. Figures 4.1 and 4.2 illustrates the orientation setup and the resulting stress map.

The simulation highlights that the stress distribution is largely uniform across the bulk of the component. As expected, stress concentrations (indicated in red) are located primarily at the interface between the supports and the component's overhanging surfaces, where the thermal gradients are most severe due to the difference in cooling rates.

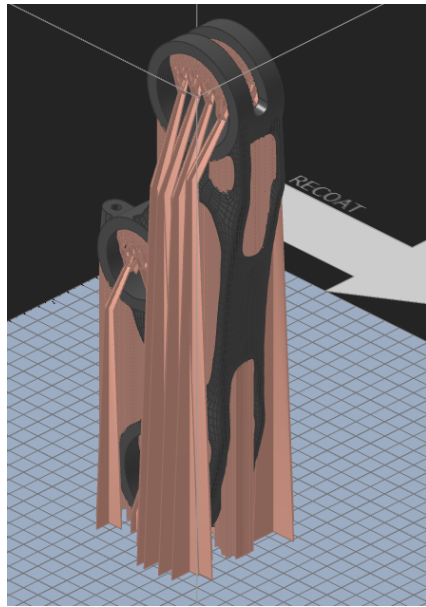


Figure 4.1: AlSi10Mg: Build orientation and support setup.

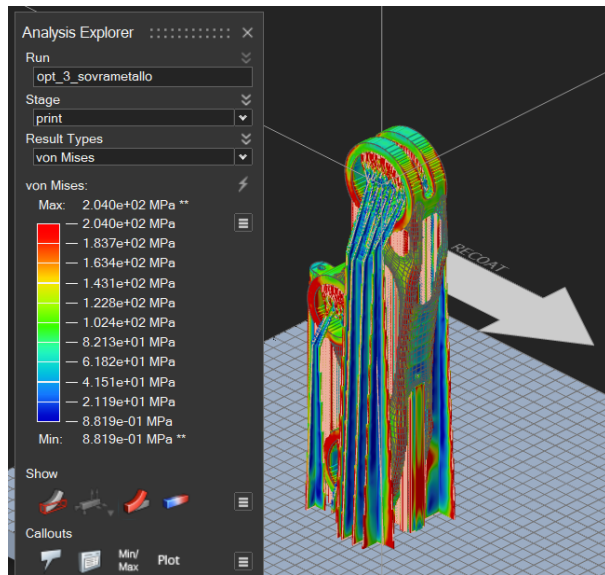


Figure 4.2: AlSi10Mg: Von Mises residual stress analysis.

4.3.2 A20X Analysis Results

The same procedural validation was applied to the high-strength aluminum alloy A20X. Given the specific mechanical properties of this material, ensuring that residual stresses do not compromise the integrity of the thin topology-optimized struts is critical. The results of the build simulation are presented in Figures 4.3 and 4.4.

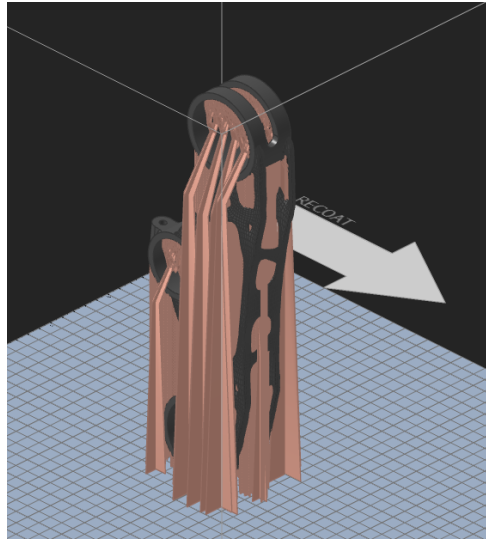


Figure 4.3: A20x: Build orientation and support setup.

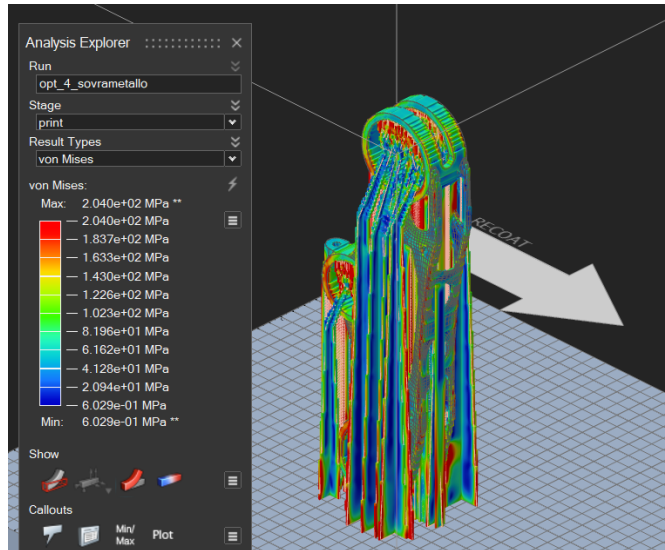


Figure 4.4: A20x: Von Mises residual stress analysis.

4.3.3 Structural Integrity Verification

The primary success criterion for this simulation is that the peak residual stresses generated during printing must remain below the yield strength ($R_{p0.2}$) of the respective materials to avoid plastic deformation or failure during the build.

The analysis provided the following peak values:

- **AlSi10Mg:** Peak Von Mises stress recorded at **204 MPa**.
- **A20X:** Peak Von Mises stress recorded at **204 MPa**.

Conclusion: In both scenarios, the red peak areas correspond to localized stress

concentrations in the support structures or at the surface skin. Crucially, these values are within the safe operating limits:

1. For **AlSi10Mg**, the typical yield strength in the as-built condition is approximately 240 – 270 MPa. The simulated peak of 204 MPa is below this threshold, ensuring the part will maintain its shape upon removal from the plate.
2. For **A20X**, known for its superior mechanical properties, the yield strength is significantly higher (> 400 MPa). Consequently, the calculated residual stress poses no risk to the structural integrity of the component.

Therefore, the simulation confirms that the defined orientation, support strategy, and process parameters are valid for manufacturing the Ducati V4S steering plate in either material without critical print failures.

Chapter 5

Performance Analysis

The methodology is the same used in section 2.5.1, the loads applied are the ones described in sections 2.1, 2.2 and 2.3.

It has to be highlighted that, in almost every case, the maximum stresses are due to the bolts pretension. The exact values will be reported in section 5.3.

5.1 FEM analysis on AlSi10Mg Part

The material card has been created with the following parameters:

Solver Keyword:	<input type="text" value="MAT1"/>
Name:	<input type="text" value="AlSi10Mg"/>
ID:	<input type="text" value="1"/>
Color:	<input type="color" value="#800000"/>
Include:	<input type="text" value="Main Model"/>
Defined:	<input checked="" type="checkbox"/>
Card Image:	<input type="text" value="MAT1"/>
User Comments:	<input type="text" value="Hide In Menu/Export"/>
E:	<input type="text" value="71000.0"/>
G:	<input type="text"/>
NU:	<input type="text" value="0.33"/>
RHO:	<input type="text" value="2.7e-09"/>
A:	<input type="text"/>
TREF:	<input type="text"/>
GE:	<input type="text"/>
ST:	<input type="text"/>
SC:	<input type="text"/>
SS:	<input type="text"/>

Figure 5.1: AlSi10Mg material card

The prepared model is shown.

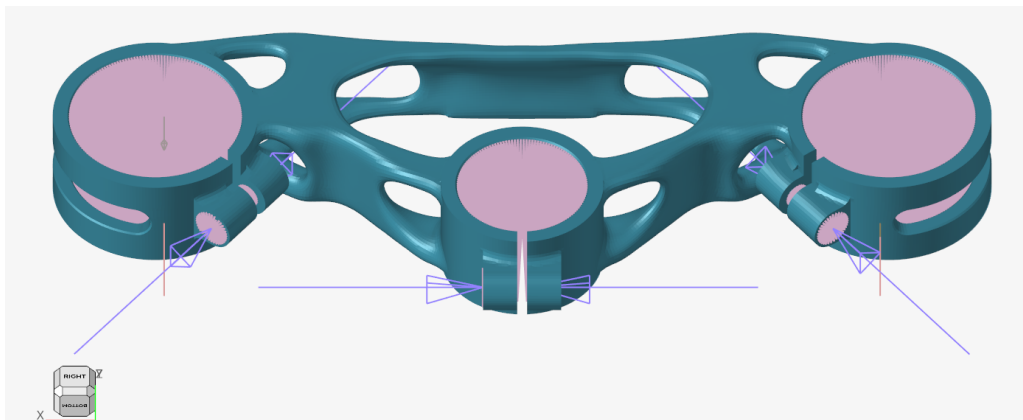


Figure 5.2: Meshed AlSi10Mg component

The results are shown.

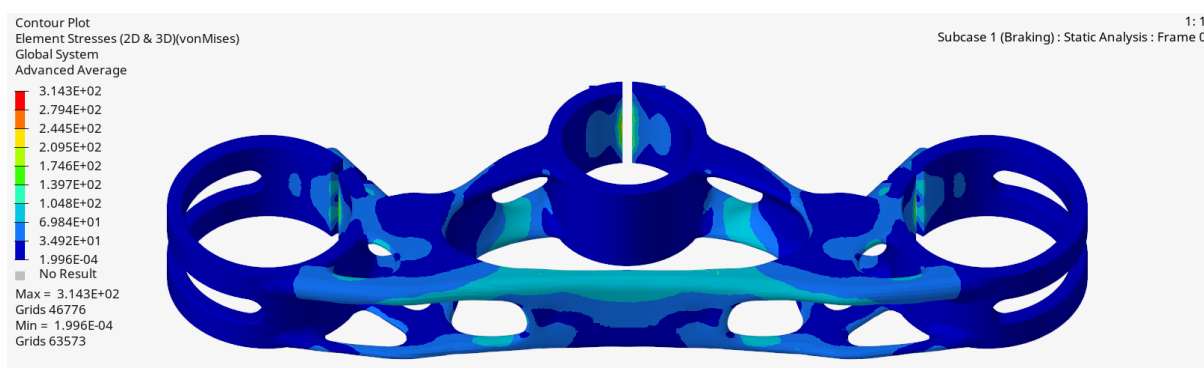


Figure 5.3: AlSi10Mg braking case (front view)

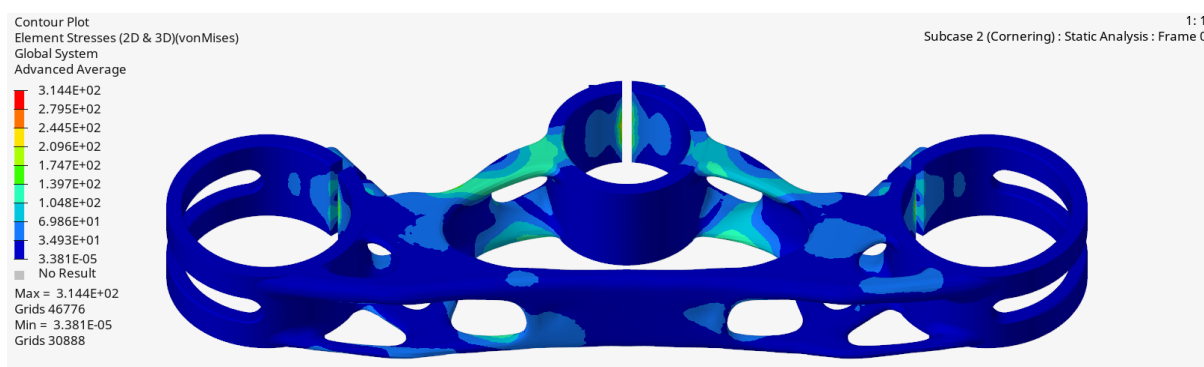


Figure 5.4: AlSi10Mg cornering case (front view)

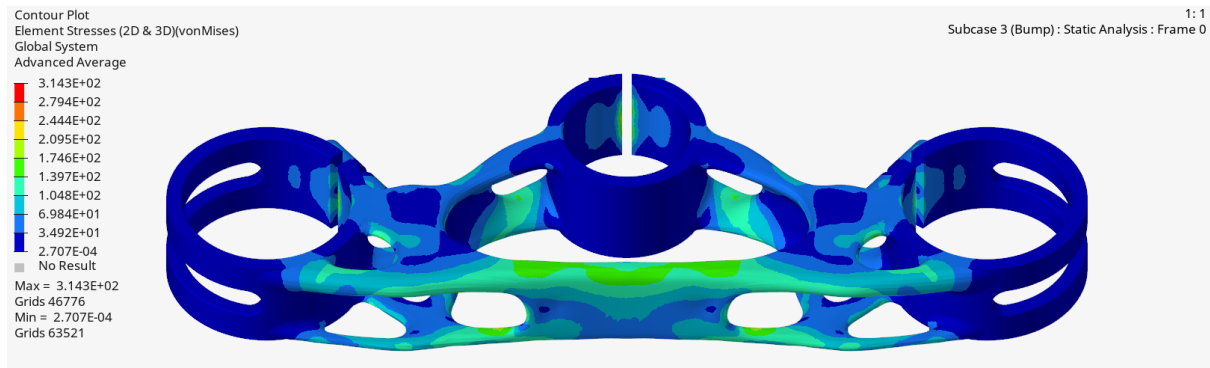


Figure 5.5: AlSi10Mg bump case (front view)

5.2 FEM analysis on A20x Part

The material card has been created with the following parameters:

Solver Keyword:	MAT1
Name:	A20x
ID:	1
Color:	
Include:	[Main Model]
Defined:	<input checked="" type="checkbox"/>
Card Image:	MAT1
User Comments:	Hide In Menu/Export
E:	77000.0
G:	
NU:	0.33
RHO:	2.85e-09
A:	
TREF:	
GE:	
ST:	
SC:	
SS:	

Figure 5.6: A20x material card

The prepared model is shown.

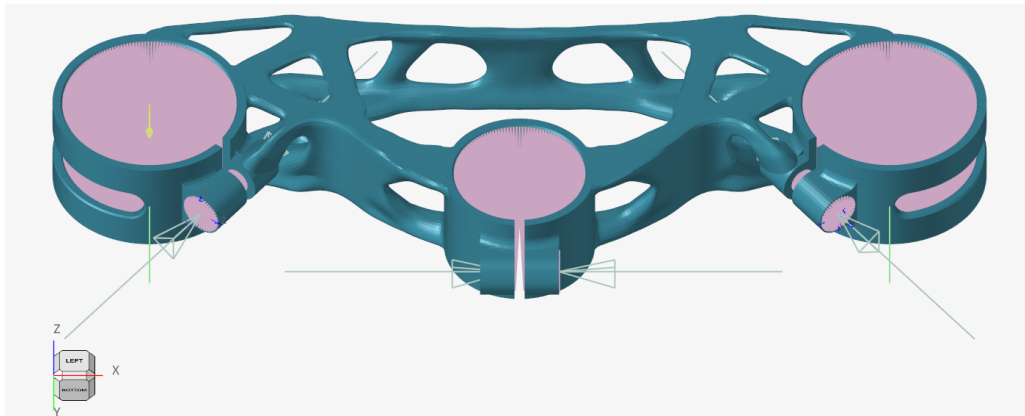


Figure 5.7: Meshed A20x component

The results are shown.

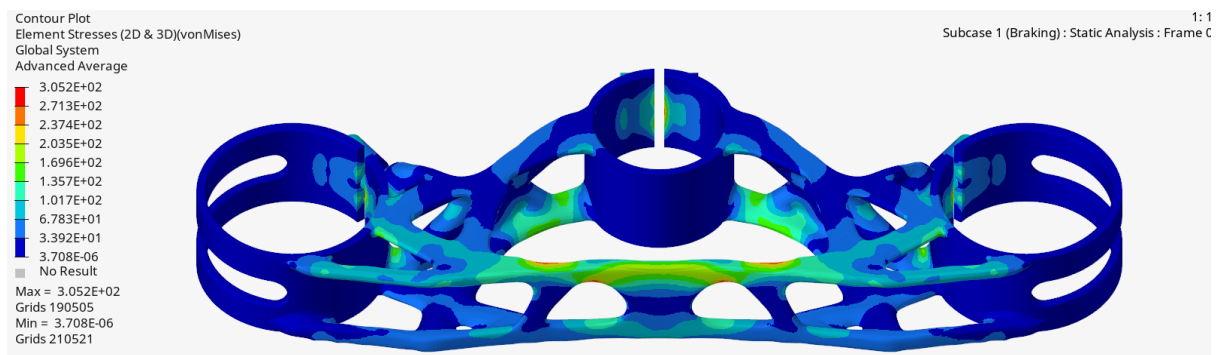


Figure 5.8: A20x braking case (front view)

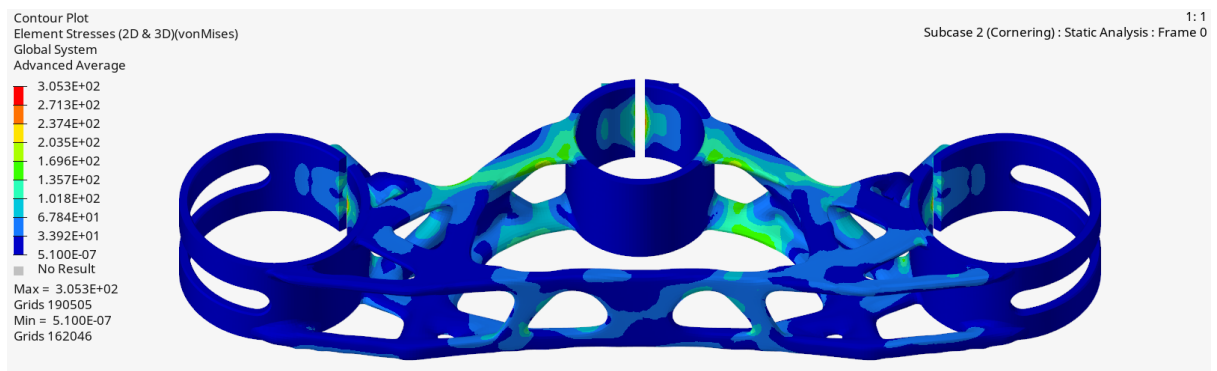


Figure 5.9: A20x cornering case (front view)

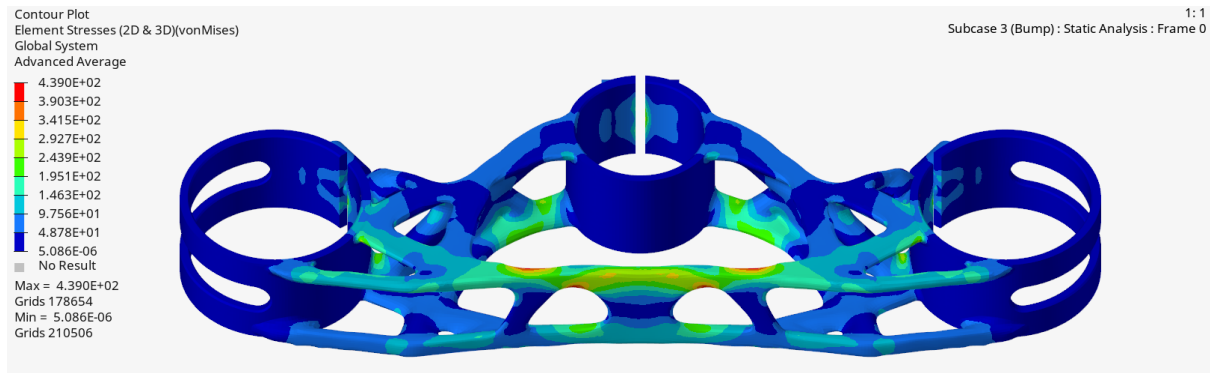


Figure 5.10: A20x bump case (front view)

5.3 FEA Results comparison

This section provides a comparative analysis of the three components across all investigated load cases. The evaluation is based on two primary parameters:

- **Safety Factor (S.F.):** Represents the margin relative to the material yielding stress $\sigma_{Rp0.2}$.
- **Stiffness:** Evaluated within two directions: lateral ($K_{b,x}$) for braking and bump cases, and vertical ($K_{b,y}$) for the cornering case.

$\sigma_{Rp0.2}$ [MPa]	σ_{max} [MPa]	S.F.	$K_{b,x}$ [$N \cdot mm$]	SF improv. [%]	
Base	260	230	1.1	1.3E+08	-
AlSi10Mg	240	125	1.9	1.7E+08	72%
A20x	440	280	1.6	1.5E+08	45%

Table 5.1: Braking case results

In the **Braking** case, the AlSi10Mg component is the clear winner, achieving the highest stiffness ($1.7 \times 10^8 N \cdot mm$) and a significant safety factor improvement of 72%. The A20x component also shows a very good result, improving the safety factor by 45% with respect to the original component.

$\sigma_{Rp0.2}$ [MPa]	σ_{max} [MPa]	S.F.	$K_{b,y}$ [$N \cdot mm$]	SF improv. [%]	
Base	260	260	1.0	1.6E+07	-
AlSi10Mg	240	140	1.7	3.2E+07	70%
A20x	440	190	2.3	2.8E+07	130%

Table 5.2: Cornering case results

In the **Cornering** case, the AlSi10Mg component achieves the highest stiffness ($3.2 \times 10^7 \text{ N} \cdot \text{mm}$) and a significant safety factor improvement of 70%. The A20x component also demonstrates excellent performance, improving the safety factor by 130% compared to the original component.

	$\sigma_{Rp0.2}$ [MPa]	σ_{max} [MPa]	S.F.
Base	260	260	1
AlSi10Mg	240	180	1.3
A20x	440	440	1

Table 5.3: Bump case results

The **Bump** load case was evaluated only for verification; all components successfully passed the test, with AlSi10Mg reaching the highest safety factor (1.3).

5.4 Weight evaluation

A mass analysis was performed to combine structural performance with weight efficiency.

Type	Density [kg/m ³]	Mass [g]	Improv. [%]
Base	2700	434	-
AlSi10Mg	2670	340	22%
A20x	2850	268	38%

Table 5.4: Mass analysis

Both Additively Manufactured components show significant weight reduction. In particular, the A20x achieves an outstanding 38% reduction (268g) thanks to its high specific strength.

5.5 Final considerations

As seen in the previous sections, the AlSi10Mg component can be declared the one with the highest overall strength, offering the highest overall stiffness in longitudinal cases.

Despite this, the A20x proved to be superior by combining the high specific strength with the reduced weight, being the lightest and still able to satisfy the safety margin.

Chapter 6

Post-Processing

Following the Additive Manufacturing process, the component requires a structured post-processing workflow to transform the as-printed raw geometry into a functional, high-precision component. This phase is critical to reconciling the organic, topology-optimized shape with the strict tolerance requirements of the Ducati V4 S assembly.

6.1 Post-Processing Strategy

The post-processing strategy is built upon four distinct pillars, defined to address the specific physical and geometrical constraints of the Laser Powder Bed Fusion (LPBF) process.

1. Heat Treatment (Stress Relief)

As predicted by the process simulation in chapter 4, the rapid cooling rates of the LPBF process induce significant residual stresses, reaching peaks of 204 MPa. To mitigate this, a stress relief annealing cycle is mandatory. This treatment is performed immediately after printing, while the components remain anchored to the build plate, to release internal tensions and prevent geometric distortion or cracking during support removal.

2. Support Removal via Custom Fixtures

Given the complex, organic morphology of the optimized design and the high production volume, manual support removal is deemed inefficient and risky. The strategy replaces manual labor with CNC machining, utilizing a series of **custom-designed fixtures** to hold the part securely while supports are milled away with high precision.

3. Abrasive Finishing

To address surface quality, abrasive finishing is employed. This operation smooths

the characteristic surface roughness of the printed part, improving both the aesthetic quality required for a visible motorcycle component and the fatigue life of the material.

4. CNC Finishing of Critical Interfaces

The functional interfaces—specifically the fork clamp housings and steering stem seat—were printed with machining allowance (as defined in section 3.4). These areas undergo CNC milling to achieve **tight tolerances**, ensuring a precise fit.

6.2 Custom Fixtures and Manufacturing Workflow

To execute the support removal and finishing strategy, a dedicated set of fixtures was engineered to securely hold the component during the process.

As detailed in chapter 3, the topology optimization results for AlSi10Mg and A20X yielded slightly different volumes and strut thicknesses due to the differing material properties. Consequently, while the *logic* of the fixtures (clamping points and orientation) remains identical, the *contact surfaces* of the AlSi10Mg fixtures were contoured specifically to match its unique geometry, ensuring the same level of stability and precision for both materials.

The implementation of this four-fixture workflow, adapted specifically for both AlSi10Mg and A20X geometries, allows for a repeatable and industrial-grade post-processing phase.

6.2.1 Operational Workflow

Fixture 1: Vertical Support Clearance

The first operation uses a vertical fixture to expose the complex internal lattice and hole features.

- **Internal Clearance:** CNC removal of the internal Tree supports located within the lower and central clamping holes.
- **Upper Feature Clearance:** Removal of the external Tree supports surrounding the upper steering stem hole.
- **Feature Definition:** Milling of the diamond supports located in proximity to the holding fixtures.

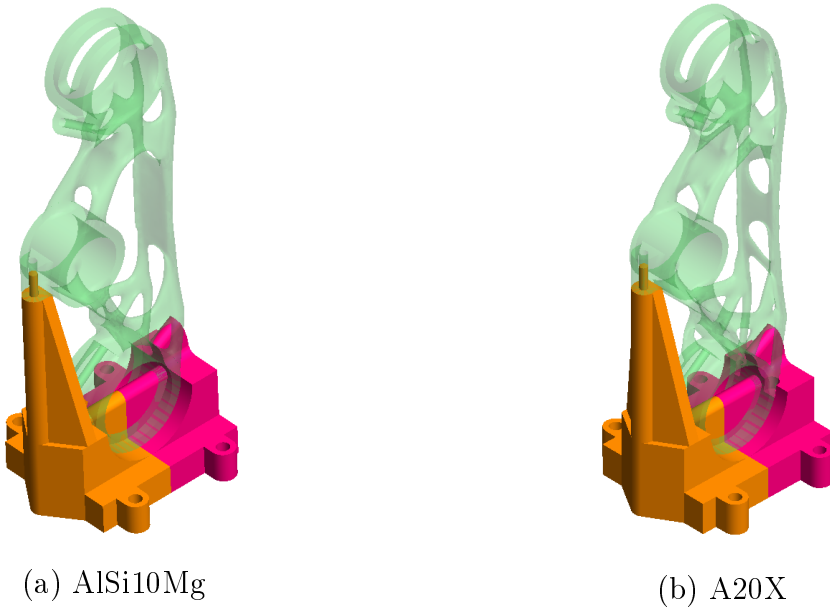


Figure 6.1: Fixture 1 for support removal

Fixture 2: Horizontal Base Removal

A dedicated fixture is employed here to mitigate part damage. Retaining the component in the previous vertical fixture for the bulk support removal would result in excessive cantilever distance, generating high bending moments and resonance frequencies during milling. Therefore, the component is transferred to a horizontal fixture to address the bulk anchors.

- **Right-Hole Clearance:** Removal of the remaining Tree support structures on the right-hand fork clamp.
- **Anchor Removal:** Milling of the massive solid supports that anchored the part to the build plate.
- **Top Access:** Removal of diamond supports accessible from the top Z-direction.

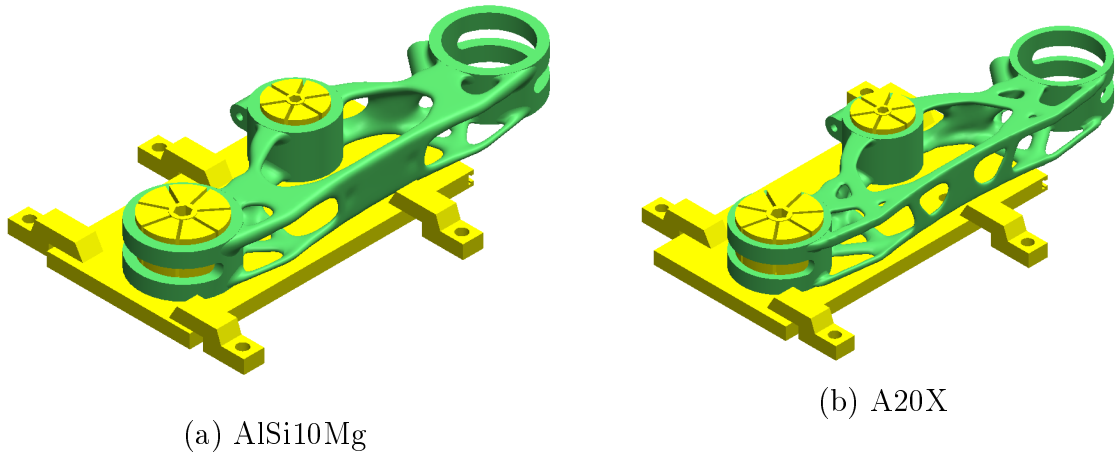


Figure 6.2: Fixture 2 for support removal

Fixture 3: Lateral Machining

A side-mounting fixture is utilized to access the bolt housing features.

- **Residual Cleanup:** Removal of any remaining diamond supports accessible from the lateral orientation.
- **Bolt Hole Threading:** Following the abrasive finishing step, this fixture is utilized to machine and thread the bolt holes, which were printed with reduced diameters.

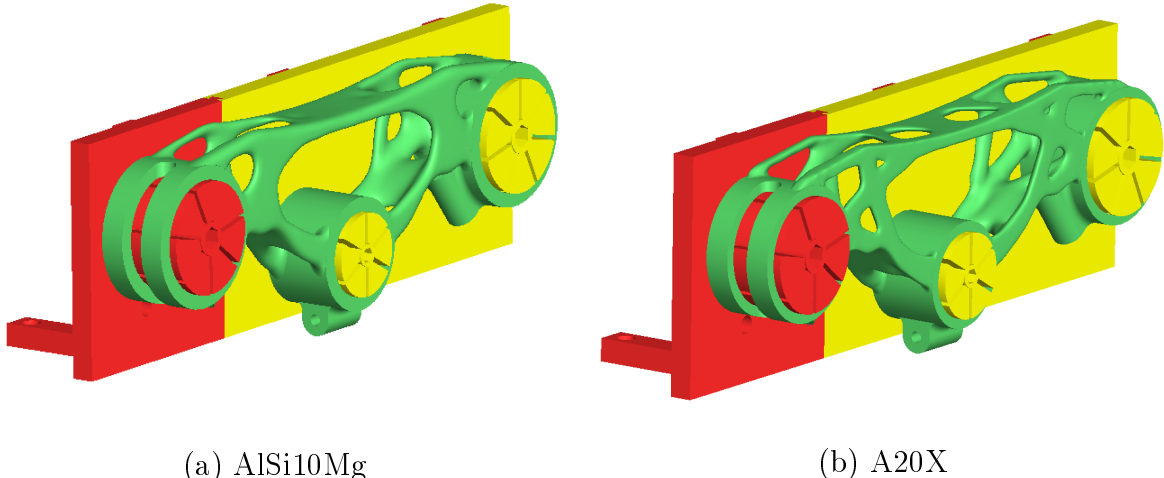


Figure 6.3: Fixture 3 for support removal and bolt holes finishing

Fixture 4: Final Tolerance Machining

The final operation employs a precision plate fixture to rigidly secure the part for high-tolerance milling.

- **Tight Tolerancing:** The machining allowance on the main clamping holes is removed to achieve the final tight fit.
- **Slot Opening:** The vertical slots on the fork clamps are machined open. This is performed as the final step to release the clamp flexibility required for function.

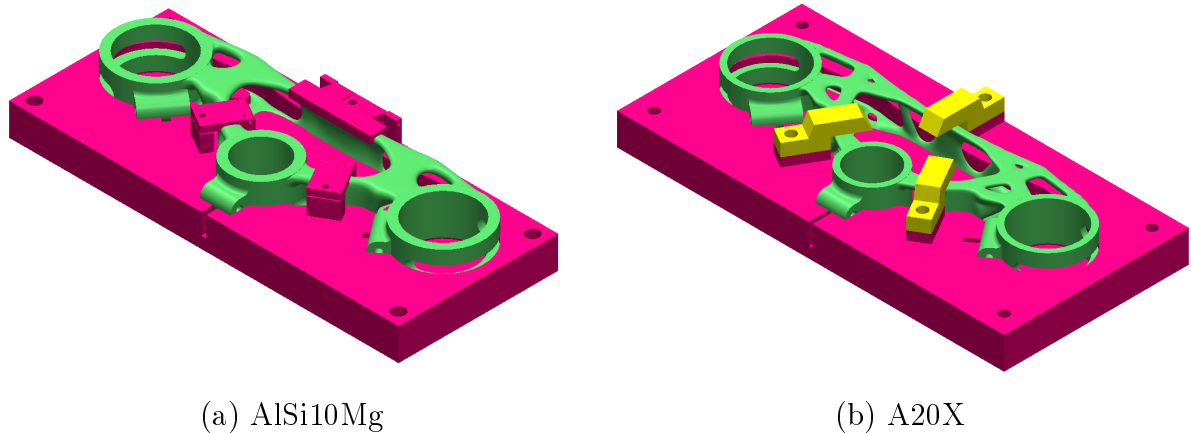


Figure 6.4: Fixture 4 for geometry finishing

Chapter 7

Cost analysis

To assess the industrial feasibility of the re-designed upper steering plate, a detailed cost analysis was conducted comparing the two selected materials: AlSi10Mg and A20X. The estimation was performed using a "Simple AM Cost Model," which breaks down the production process into four main cost drivers: Design, Set-up, Building, and Post-processing/Finishing.

The analysis is based on a projected production volume of 500 parts. The manufacturing process assumes the use of an EOS M 400-4 system, a large-frame industrial machine suitable for series production.

The following fixed parameters and assumptions were applied to both material cases to ensure a consistent comparison:

- Machine Hourly Rate: 230 €/h (inclusive of amortization, maintenance, and energy consumption).
- Nesting Strategy: 12 parts per build job (optimized for the EOS M 400 platform).
- Set-up Time: 180 minutes per job, accounted at a professional rate of 30 €/h.
- Finishing Cost: Estimated at 80 € per part. It is important to note that this figure includes not only the CNC machining of the critical interfaces (bearing seats and fork clamps) but also the costs associated with producing the necessary custom fixtures and soft jaws. These auxiliary components (Figures 6.1, 6.2, 6.3, 6.4) are essential to rigidly clamp the complex, organic AM geometry during the subtractive finishing stages.

For the calculation of the "Part + Support Volume," a conservative simplification was made. The support structures were modeled with the same density as the solid component. In a real-world manufacturing scenario, these supports would be generated

with a significantly lower effective density. Consequently, the material consumption and laser exposure time presented in this model are slightly overestimated, meaning the actual production cost would likely be lower than the figures reported below.

The total production cost per part (CPP) was calculated for both the standard aluminum alloy (AlSi10Mg) and the high-performance alloy (A20X). The results are summarized in Tables 7.1 and 7.2.

	Cost
Design cost	0.24 €
Set-up cost (per part)	7.50 €
Building cost (per part)	477.44 €
Post-processing cost (per part)	40 €
Finishing cost	80 €
Total	605.18 €

Table 7.1: AlSi10Mg case

	Cost
Design cost	0.24 €
Set-up cost (per part)	7.50 €
Building cost (per part)	467.57 €
Post-processing cost (per part)	40 €
Finishing cost	80 €
Total	595.31 €

Table 7.2: A20x case

- AlSi10Mg (Standard Case): As shown in Table 7.1, the total cost for the AlSi10Mg component is 605.18 €. The most significant cost driver is the Building Cost (477.44 €), which accounts for approximately 79% of the total price. This is driven largely by the machine running time required to melt the component's volume.
- A20X (High-Performance Case): Table 7.1 presents the cost breakdown for the A20X component, resulting in a total cost of 595.31 €. Despite A20X being a premium material with significantly higher raw powder costs (130 €/kg vs. 75 €/kg for AlSi10Mg) and higher inert gas consumption costs (24 €/m³ vs. 6 €/m³), the final part is surprisingly cheaper.

A comparative analysis reveals a counter-intuitive result: the high-performance material (A20X) is more economical than the standard material. This phenomenon can be explained by examining the interaction between topology optimization and process parameters.

The superior mechanical properties of A20X (specifically its higher yield strength) allowed the topology optimization algorithm to remove more material while maintaining structural integrity. The optimized volume (part + supports) for the A20X job is approximately 160 cm³, compared to 200 cm³ for the AlSi10Mg job.

In Additive Manufacturing, machine time is the dominant cost factor. The reduction in printed volume for the A20X design translated directly into a shorter laser scanning time. The total Job Time was reduced from 22.3 hours (AlSi10Mg) to 20.2 hours (A20X).

The savings generated by reducing the machine time (approx. 2 hours per job at 230 €/h) outweighed the increased costs of the raw A20X powder and the specialized inert gas required for processing it.

So, in conclusion, the economic analysis demonstrates that transitioning to a high-performance material like A20X does not necessarily incur a higher unit cost. On the contrary, the "lightweighting" potential of the material enables a more aggressive topology optimization, which reduces the volume to be printed.

For this specific application, A20X is the superior choice, offering a lighter component (better performance) at a slightly lower production cost (595.31 € vs. 605.18 €), validating the economic viability of the high-performance re-design.

7.1 Production Rate and Lead Time Assessment

The industrialization strategy considers a continuous production flow optimized for the EOS M 400 system capabilities. Based on the A20X simulation results, the total turnover time per job fits approximately within a 24-hour cycle. With a nesting density of 12 parts per job, the manufacturing cell achieves a daily output of 12 components.

Operating on a standard 5-day working week, this results in a steady throughput of 60 parts per week. Consequently, to fulfill the complete order of 500 units, the estimated lead time is approximately 9 weeks. This projection accounts for the nominal production rate while including a necessary safety margin to manage potential non-conformities, routine machine maintenance, or operational delays. Additionally, the amortization of the initial design and pre-production setup phases impacts the final price by 7.74 €/part, a value that benefits significantly from this high-volume serial production approach.

Chapter 8

Conclusion

This report presented a comprehensive feasibility study regarding the transition of the Ducati V4 S upper steering plate from traditional CNC machining to an Additive Manufacturing workflow. By integrating topology optimization, process simulation, and economic analysis, the study confirms that adopting Additive Manufacturing for this component is not only technically feasible but highly advantageous compared to conventional subtractive methods.

The structural and geometric analysis highlighted the critical role of material selection in maximizing the potential of generative design. While both AlSi10Mg and A20X alloys were validated against the rigorous dimensioning load cases (including braking, cornering, and bump impacts) the A20X alloy emerged as the superior candidate. Its exceptional yield strength allowed for a more aggressive topology optimization strategy, enabling a significant reduction in wall thickness and overall volume without compromising structural integrity or stiffness.

From a manufacturing perspective, the simulation of the printing process on the EOS M 400-4 system successfully validated the production strategy. The proposed vertical orientation, combined with a hybrid support structure, proved effective in managing residual stresses, keeping them well below the yield threshold for both materials. Furthermore, the post-processing workflow defined in this study ensures that the tight tolerances required for the steering assembly are consistently met.

The economic assessment provided the most decisive argument for the final selection. Contrary to standard assumptions, the use of the high-performance A20X material resulted in a lower cost per part (595.31 €) compared to the standard AlSi10Mg (605.18 €). This counter-intuitive result is driven by the "lightweighting" capability of A20X: the reduced material volume translates directly into shorter laser exposure times, significantly cutting machine running costs which outweigh the higher price of the raw powder.

In conclusion, the project identifies a unique "Win-Win" scenario: the re-designed

A20X component is simultaneously lighter, mechanically superior, and more economical to manufacture than its standard aluminum alloy counterpart. Therefore, based on the verified mechanical performance and the favorable cost analysis, the adoption of the A20X alloy is strongly recommended for the serial production of the Ducati V4 S steering plate.